Appl Phys B (2011) 104:805–811
DOI 10.1007/s00340-011-4675-0

Applied Physics B
Lasers and Optics

Trends and trade-offs in nematicon propagation

A. Piccardi · M. Trotta · M. Kwasny · A. Alberucci · R. Asquini · M. Karpierz · A. D'Alessandro · G. Assanto

Received: 29 April 2011 / Revised version: 20 June 2011 / Published online: 30 July 2011

Abstract We investigate the propagation of nematicons in various nematic liquid crystals. Following some general considerations on the role of material parameters in light self-trapping via a reorientational nonlinear response, we discuss numerical results on light self-action and transverse localization. Finally, we validate our findings with experimental measurements in three liquid crystalline mixtures featuring different amounts of birefringence.

1 Introduction

With the invention of the laser, available light intensities have become high enough to allow observing nonlinear effects and, among them, self-focusing. The latter occurs when the beam phase-fronts bend in such a way as to counteract diffractive spreading [1]. When self-focusing balances diffraction, a spatial soliton is generated, i.e., a wave-packet retaining its shape in propagation [2, 3]. In centrosymmetric media the simplest nonlinear response is modeled by changes in refractive index n proportional to the local intensity I, i.e. $\Delta n = n_2 I$, with n_2 the Kerr coefficient [4]. Therefore, a bell-shaped beam can give rise to a guiding transverse index profile [5, 6], eventually resulting in a bright spatial soliton. Spatial solitons in Kerr media are stable only in $(1+1)$D geometries [7, 8] (i.e., with diffraction taking place only in one transverse dimension, for instance in slab waveguides), but undergo filamentation and catastrophic collapse in $(2+1)$D geometries (i.e., diffraction acting in both transverse dimensions). The first observations of spatial solitons with cw lasers in $(2+1)$D were reported by Dabby and co-workers in lead glasses [9] and by Bjorkholm and co-workers in sodium vapors [10], respectively: in these experiments, the stabilization of the self-trapped beam was provided by either a nonlocal response in the former case [11] or by saturation in the latter. Nonlocal nonlinear media feature an index well Δn wider than the intensity profile I, with the size of nonlocality depending on the width ratio of Δn and I. Typically, nonlocality can be ascribed to diffusive processes, such as heat transfer [9, 12], molecular/atomic diffusion [11], electrostriction [13], thermophoresis [14], diffraction [15] and long-range intermolecular links, as in nematic liquid crystals (NLC) [16, 17]. In the area of light self-localization, NLC have attracted a great attention because of their unique dielectric properties: large nonlinearity and spectral transparency [18], highly nonlocal response [19] and large tunability (linear as well as nonlinear) via external perturbations, e.g. quasi-static or optical frequency electric fields [20]. Liquid crystals consist of organic molecules with intermediate properties between solids and liquids. The nematic phase is usually characterized by a high degree of orientational order, with the average direction of the major molecular axis described by a vector field named director $\hat{n}$ [18, 21]; conversely, no long-range positional order is present. With reference to their linear optical properties, NLC are uniaxials with the optic axis along $\hat{n}$, refractive indices $n_{||}$ and $n_{\perp}$ for electric field parallel and nor-

A. Piccardi · A. Alberucci (✉) · G. Assanto
Nonlinear Optics and OptoElectronics Lab (NooEL), University of Rome "Roma Tre", Via della Vasca Navale 84, 00146 Rome, Italy
e-mail: alberucc@uniroma3.it

M. Trotta · R. Asquini · A. D'Alessandro
Dipartimento di Ingegneria dell'Informazione, Elettronica e Telecomunicazioni, University of Rome "Sapienza", Via Eudossiana 18, 00184 Rome, Italy

M. Kwasny · M. Karpierz
Faculty of Physics, Warsaw University of Technology, Koszykowa 75, 00-662 Warsaw, Poland

mal to $\hat{n}$, respectively. The peculiar nonlinear mechanism in NLC is then reorientational: an electric field induces dipoles in the nonpolar molecules and tends to align them in order to minimize the energy [18, 21]. Reorientational spatial solitons in NLC, often called nematicons [17, 22], were reported in slab waveguides [23], in planar cells with $\hat{n}$ pre-tilted via a bias (to avoid the Freedericksz threshold) [24], in unbiased planar cells [25], in arrays of coupled waveguides [26, 27] and in chiral NLC [28, 29]. Light self-localization through thermal effects in cylindrical structures (capillaries) was also observed [30], as well as the interplay between thermal and reorientational responses [31]. Moreover, localization was reported in the form of modulationally unstable patterns in nematic liquid crystals with coherent [25, 32–35] and spatially incoherent excitations [36], as well as dark solitons in self-defocussing mixtures [37].

Nematicons possess several interesting properties: they can be excited at input powers of mW due the large nonlinearity (even well below mW in doped NLC [38]), can guide probes of different wavelengths or even incoherent light [39–41], can be steered via an additional voltage bias [20, 25, 42]. Their intrinsic robustness permits their interaction with defects without losing self-trapping: large angle deflections were demonstrated via refraction/reflection at interfaces (created by voltage [43] or by an external light beam [44–46]), with all-optically induced perturbations [47–49], and with air bubbles [50]. Individual nematicons can self-act on their trajectory by changing the walk-off [51] or undergoing a transverse force [52]. All-optical logic/switching gates based upon these phenomena have been demonstrated [44, 53].

All the properties summarized above make nematicons ideal candidates for the realization of all-optical signal processing microsystems; to this extent it is crucial to understand the role of specific NLC properties towards applications. In this paper we study, both theoretically and experimentally, the propagation of individual nematicons in NLC with various dielectric properties. We will show theoretically that, for a given initial distribution of $\hat{n}$, the nonlinear response depends on the linear refractive indices $n_{||}$ and $n_{\perp}$ and on the magnitude of the forces binding the molecules to one another. We will discuss the dominant role of the anisotropy $\epsilon_a = n_{\parallel}^2 - n_{\perp}^2$ and validate our results using a (1 + 1)D simulator. We confirm our findings by the experimental observation of light self-trapping in three NLC mixtures with different degrees of optical anisotropy, i.e. birefringence.

2 Model

Let us consider a planar cell as sketched in Fig. 1. An NLC layer of thickness L is confined between two parallel glass

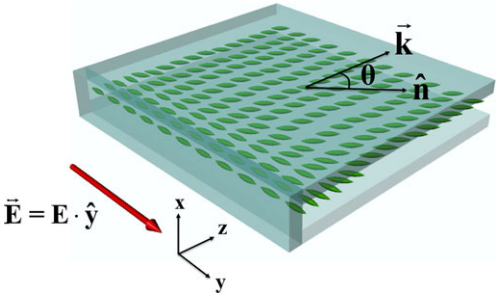

Fig. 1 Sketch of a planar cell. The *green ellipses* represent the NLC molecules. The interfaces parallel to yz are located in $x = 0$ and $x = L$, respectively, i.e., L is the cell thickness

slides, with the x axis normal to them; the glass/NLC interfaces are treated to ensure that $\hat{n}$ lies in the plane yz in their proximity, at an angle θ_0 with $\hat{z}$. A third glass slide seals the cell, with $\hat{n}$ aligned parallel to $\hat{y}$ in order to maximize the input electric field coupling to an extraordinary wave in the bulk NLC [54]. A transition zone for $0 < z < L$ connects the input interface to the bulk NLC: we will neglect its effects as we are interested in light propagation in the volume of the cell, assuming the director to be uniformly distributed in the sample. Finally, we will consider the cell infinitely extended along y. The sample is excited by a TEM_{00} beam at wavelength λ with wave vector $\boldsymbol{k}$ along $\hat{z}$, polarized along y to couple into the extraordinary wave in bulk (ordinary waves are subject to the Freedericksz threshold; hence, they are not suited for the exploitation of reorientation towards self-localization [18, 21]). We consider in $z = 0$ a flat phase-front and a beam waist w_0, i. e., an electric field of the form $\boldsymbol{E}(x, y, z = 0) \propto \hat{y} \exp[-(x^2 + y^2)/w_0^2]$. We define $\theta = \theta_0 + \psi$, with θ the angle between $\hat{n}$ and $\hat{z}$ [i.e. $\hat{n} = (0, \sin\theta, \cos\theta)$], accounting for the action of the electromagnetic torque with the optical perturbation ψ on the director distribution in angle. The components of the dielectric tensor $\boldsymbol{\epsilon}$ can be expressed as $\epsilon_{jl} = \epsilon_{\perp}\delta_{jl} + \epsilon_a n_j n_l$ $(j, l = x, y, z)$, where $\epsilon_a = n_{\parallel}^2 - n_{\perp}^2$ is the optical anisotropy, $n_j = \hat{j} \cdot \hat{n}$ and δ_{jl} is the Kronecker's delta; hence, it is clear that the linear properties of the system depend only on $n_{\parallel}, n_{\perp}$ and θ_0. Naming H the extraordinary component of the magnetic field parallel to $\hat{x}$ and setting $H = A \exp(ik_0 n_0 z)$ [$k_0 = 2\pi/\lambda$ is the vacuum wavenumber and $n_0 = (\cos^2\theta_0/n_{\perp}^2 + \sin^2\theta_0/n_{\parallel}^2)^{-1/2}$], light propagation in the paraxial perturbative regime is ruled by [51, 55]

$$2ik_0 n_0 \left(\frac{\partial A}{\partial z} + \tan\delta_0 \frac{\partial A}{\partial y}\right) + D_y \frac{\partial^2 A}{\partial y^2} + \frac{\partial^2 A}{\partial x^2} + k_0^2 \Delta n_e^2 A = 0, \quad (1)$$

$$\nabla^2 \psi + \gamma\kappa^2 \sin\big[2(\theta_0 + \psi - \delta_0)\big]|A|^2 = 0, \quad (2)$$

where we defined the extraordinary refractive index (profile) $n_e = (\epsilon_{yy} - \epsilon_{yz}^2/\epsilon_{zz})^{1/2}$ [Fig. 2(a)] and the nonlinear index well $\Delta n_e^2 = n_e^2 - n_0^2$ [note that $n_0 = n_e(\theta_0)$], the walk-off angle $\delta_0 = \arctan[\epsilon_a \sin 2\theta_0/(\epsilon_a + 2n_\perp^2 + \epsilon_a \cos 2\theta_0)]$ [Fig. 2(c)] and the diffraction coefficient $D_y = n_0^2/\epsilon_{zz}(\theta_0)$; we also introduced the light-matter coupling $\gamma = \epsilon_0\epsilon_a/(4K)$ (K is the Frank's elastic constant taken to be the same for bend, twist and splay deformations [21]) and $\kappa = -Z_0/(n_0 \cos\delta_0)$ (Z_0 is the impedance of vacuum), which links electric and magnetic fields of the lightwave [55]. Equation (1) is a nonlinear Schrödinger-like equation accounting for anisotropy (including walk-off) and nonlocality (via Δn_e^2), whereas (2) states the equilibrium between the torque due to intermolecular forces (Laplacian term) and the torque due to the optical field (a term dependent on $|A|^2$) [16, 18, 21]; noticeably, (2) is a diffusion equation because the perturbation induced by light (Δn_e^2) spreads out in NLC due to strong interactions between molecules, as noted in Sect. 1.

Equation (2) rigorously holds valid when $K_1 = K_3$ (K_1 and K_3 are the elastic constants for splay and bend deformations, respectively [21]), with an effective K given by an average of all three constants; when $K_1 \neq K_3$, extra terms depending on the first partial derivatives of θ and on the mixed second-order derivative appear. Nevertheless, our measurements indicate that the single constant approximation is valid finely, with good agreement between data and model when K is determined via a best fit procedure [55].

Setting $A = \sqrt{P}u$ with P the beam power, from (2) it is apparent that, for a given optical field, the nonlinear index perturbation depends on the parameter $\sigma = \gamma\kappa^2 P$. Let us consider two NLC mixtures with the same (unperturbed) angle θ_0 and refractive indices $n_\perp$ and $n_\parallel$, but with different elastic constants K^I and K^{II}, respectively: a normalized input field $u_0 = u(x, y, z = 0)$ will undergo the same evolution in propagation if $P^I = (K^I/K^{II})P^{II}$, with P^I and P^{II} the beam powers corresponding to the mixtures with K^I and K^{II}, respectively.

We first consider the linear case, i.e., $\Delta n_e^2 = 0$; the input Gaussian beam will evolve according to the Helmholtz's (paraxial) equation, with

$$A = \frac{\sqrt{P}}{w(z)}\sqrt{\frac{2n_0\cos\delta_0}{\pi Z_0}}e^{i\zeta}e^{[i\frac{k_0 n_{\rm eff}}{2R(z)} - \frac{1}{w^2(z)}][x^2 + (y - z\tan\delta_0)^2]}, \quad (3)$$

where we introduced the effective index $n_{\rm eff} = n_0/D_y$ [Fig. 2(b)], the Rayleigh distance $l_R = \pi w_0^2 n_{\rm eff}/\lambda$, the Gouy phase $\zeta = \arctan(z/l_R)$, the spot size $w(z) = w_0\sqrt{1 + (z/l_R)^2}$ and the curvature radius $R(z) = z[1 + (l_R/z)^2]$. The divergence ϕ of the beam is $\phi = \lambda/(\pi w_0 n_{\rm eff})$: hence, the beam diffraction depends both on the NLC indices and on the director angle θ_0. Specifically, fixing beam waist w_0 and index $n_\perp$, after setting $n_{\rm eff}(\theta_0, \epsilon_a) = n_\perp/D_y|_{\epsilon_a=0} + \delta n$ (δn quantifies changes in $n_{\rm eff}$ due to the anisotropy) it is straightforward to compute the variations $\Delta\phi$ in divergence,

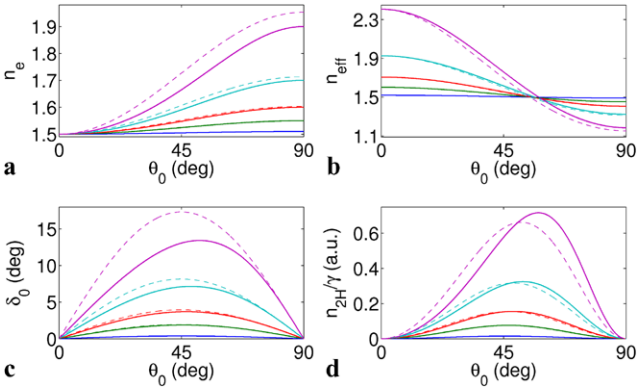

Fig. 2 Plots versus θ_0 and for $\Delta n = 0.01, 0.05, 0.1, 0.2, 0.4$ (*bottom* to *top lines*): (**a**) the extraordinary index n_e, (**b**) the effective index $n_{\rm eff}$, (**c**) the walk-off δ_0 and (**d**) the ratio between the nonlocal Kerr coefficient n_{2H} and the material-dependent parameter γ. *Solid lines* are exact values, *dashed lines* approximated values for small anisotropies ϵ_a. Here $n_\perp = 1.5$

$$\Delta\phi = -\frac{\lambda}{\pi w_0}\frac{\delta n}{n_\perp^2}, \quad (4)$$

which implies that the beam divergence decreases with higher $n_{\rm eff}$, consistently with (3). Thus, when comparing light self-localization in various NLC (i.e., different ϵ_a), the differences in diffraction have to be accounted for. For instance, Fig. 2(b) provides $\delta n = 0.26$ for $\theta_0 = 45°$, $n_\perp = 1.5$ and $\Delta n = 0.4$, i.e. $\Delta\phi = -0.7°$ on a divergence $\phi = 4°$ for $\epsilon_a = 0$, a relative change of the order of 20%.

After linearizing Δn_e^2 (i.e., $\Delta n_e^2 \approx 2n_0\Delta n_e$), from (1)–(2) we can define a nonlocal effective Kerr coefficient n_{2H} [55]:

$$n_{2H}(\theta_0) = 2\gamma\kappa^2 \sin\big[2(\theta_0 - \delta_0)\big]n_e^2(\theta_0)\tan\delta_0. \quad (5)$$

Equation (5) includes the dependence of self-focusing on the director distribution at rest (i.e., θ_0) [55] and on the material parameters through the birefringence ϵ_a and the elastic constant K. The Kerr coefficient n_{2H} is inversely proportional to K as large elastic constants correspond to higher powers in order to get the same all-optical reorientation ψ; in addition, n_{2H} is approximately proportional to the square of the optical anisotropy ϵ_a as the latter is in turn proportional to the induced torque for a fixed excitation [see (2)] and the nonlinear index well depends on ϵ_a for a given perturbation ψ [see Fig. 2(a)].

To quantitatively address the dependence of the nonlinearity, we first analyze the case of small anisotropy; in this limit we can write

$$n_e = n_\perp + \frac{\sin^2\theta_0}{2n_\perp}\epsilon_a, \quad (6)$$

$$\delta_0 = \frac{\sin 2\theta_0}{2n_\perp^2}\epsilon_a, \tag{7}$$

$$n_{2H} = \frac{\epsilon_0 \kappa^2}{4K}\epsilon_a^2 \sin\big[2(\theta_0 - \delta_0)\big]\sin(2\theta_0). \tag{8}$$

Figure 2 shows the comparison between the exact formula and the results stemming from (6)–(8). For anisotropy up to $\Delta n = n_\parallel - n_\perp < 0.1$ and for $n_\perp = 1.5$, the agreement between full and approximated expressions is excellent, whereas for larger Δn (lines for $\Delta n = 0.2$) slight differences appear; in particular, the maxima in walk-off δ_0 and Kerr coefficient n_{2H} shift towards θ_0 larger than 45° as the anisotropy increases.

Looking at (8) it is clear that the nonlinear effects, for given θ_0 and elastic constant K, depend on the square of ϵ_a. This result is valid for small ϵ_a; for large anisotropies the behavior is more involved, although the qualitative trend remains valid, with a shift of the director angle corresponding to the maximum nonlinearity as the plots of Fig. 3 show.

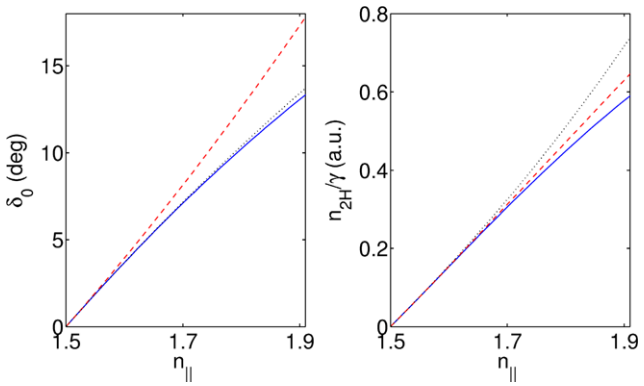

Fig. 3 (*Left*) Walk-off δ_0 and (*right*) Kerr coefficient n_{2H}/γ versus $n_\parallel$ for $\theta_0 = 45°$ from the exact formula (*solid lines*) and in the limit of small optical anisotropy (*dashed lines*). The *dotted lines* are the corresponding maxima versus θ_0 calculated exactly for each $n_\parallel$. Here $n_\perp = 1.5$

3 Numerical simulations

3.1 (1 + 1)D model

The numerical integration of the system of (1)–(2) is time-consuming, as it requires the iterative solution of a boundary problem in a 3D geometry. A simplified (1 + 1)D model can be obtained from (1)–(2) when assuming light propagation in the cell mid-plane $x = L/2$ (i.e., no boundary effects [56]) and studying beam evolution in the plane yz (notably, in typical experiments only the light distribution in yz is acquired by imaging the NLC scattered photons out of the plane [24, 57]). Setting $A = X(x,z)v(y,z)$ and $\psi = \varphi(y,z)\sin(\pi x/L)$, (1)–(2) in $x = L/2$ provide [51, 55]:

$$2ik_0 n_0\left(\frac{\partial v}{\partial z} + \tan\delta_b \frac{\partial v}{\partial y}\right) + D_y \frac{\partial^2 v}{\partial y^2} + k_0^2 \Delta n_e^2 v + 2i\alpha k_0 n_0 v = 0, \tag{9}$$

$$\nabla_{yz}^2 \varphi - \left(\frac{\pi}{L}\right)^2 \varphi + \gamma\kappa^2 \sin\big[2(\theta_0 + \varphi - \delta_0)\big]|v|^2 = 0, \tag{10}$$

with the last term in (9) accounting for scattering losses, always present in the nematic phase. In (9) we also included self-steering via nonlinear changes in walk-off by setting $\delta_b = \delta(\theta_0 + \psi_b)$, with ψ_b the maximum all-optical perturbation for z constant [51, 55, 58]. The reorientation equation (10) is a screened Poisson equation with screening length L, i.e. conserving the nonlocality of the real 3D system, determined by the shortest size of the cell, i.e. the thickness L [59]. Finally, the power in the simplified (1 + 1)D model [see (9)–(10)] P_{2D} is smaller than the actual one P, that is, $P = \eta P_{2D}$ with typical η in the range $3 \div 10$ [51, 55]. The system of (9)–(10) is solved iteratively: for a given $\boldsymbol{\epsilon}$ the beam propagation is computed via (9), then the new field is

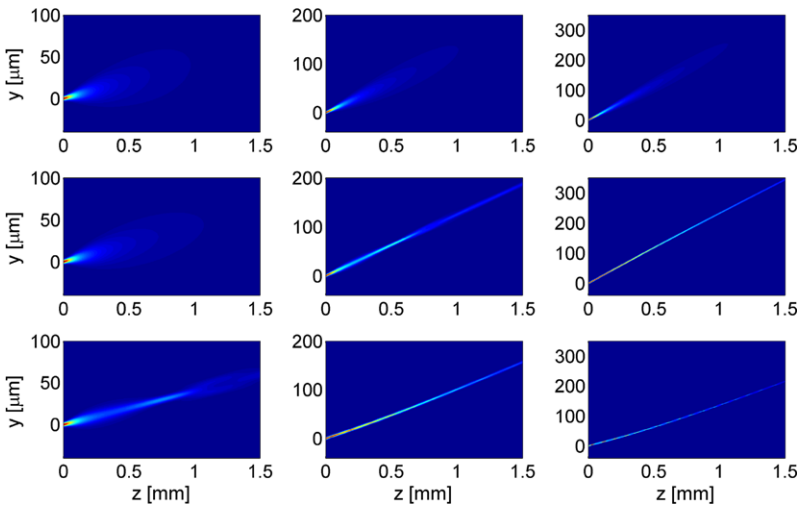

Fig. 4 Beam profile $|v|^2$ computed from (9)–(10). *First*, *second* and *third columns* (*rows*) correspond to $\Delta n = 0.06, 0.2, 0.4$ ($P_{2D} = 1$ μW, 0.5 mW, 4 mW), respectively. Here $w_0 = 3$ μm, $\lambda = 1064$ nm, $L = 75$ μm, $n_\perp = 1.5$, $K = 12$ pN and the attenuation (scattering losses) is $\alpha = 5$ cm^{-1}

used in (10) to calculate the variations in director distribution induced by the new perturbation; the cycle is repeated until convergence is achieved.

3.2 Results

Figure 4 shows the computed light evolution in the plane $x = L/2$. As predicted in Sect. 2, for a fixed input power the larger is the NLC anisotropy the stronger is self-focusing (compare different columns); accordingly, the power required for self-trapping drops for large ϵ_a. The anisotropy also affects the soliton trajectory via walk-off (note the different ranges of y in each column of Fig. 4), consistently with Fig. 2(c). At high powers the optical reorientation is large enough to change the soliton trajectory via nonlinear walk-off, with sideway displacements of dozens of microns in $z = 1.5$ mm at 4 mW (bottom row in Fig. 4).

Figure 5 plots waist w and trajectory (defined as the first and second central moments of the distribution $|v|^2$, respectively). The trajectories in the linear regime depend on δ_0, with larger walk-off angles for larger anisotropies [see Fig. 2(c)]; the anisotropy affects diffraction as well, with beam spreading decreasing with Δn [see (4)]. In the nonlinear regime the soliton trajectory for small anisotropies does not appreciably vary for powers up to 4 mW (in the scale of Fig. 5 linear and nonlinear trajectories overlap for $\Delta n = 0.06$), whereas self-deflection becomes appreciable for large birefringence even at these excitations. Owing to losses, beam breathing in waist changes in propagation, both in amplitude and period [51, 55]. To quantify the nonlinear effects, we introduce the mean beam waist $\overline{w}$ as

$$\overline{w} = \frac{1}{L_z} \int_0^{L_z} w(z)\, dz. \tag{11}$$

The behavior of $\overline{w}$ versus power P_{2D} in $L_z = 1.5$ mm is plotted in Fig. 5: clearly the power required for self-confinement is lower for larger ϵ_a. Noteworthy, $\overline{w}$ saturates with excitation, in agreement with the nematicon existence curve versus waist and power in the absence of losses, i.e. $P \propto w^{-2}$ [19, 51].

4 Experimental results

To validate the theoretical and numerical results as reported in Sects. 2–3, we fabricated three planar glass cells of thickness $L = 75$ μm (Fig. 1), and filled them with distinct NLC mixtures, namely 1550, $E7$ and $1791A$ [60, 61]. A TEM_{00} Gaussian beam at $\lambda = 1064$ nm was coupled into the NLC samples using a microscope objective, with an input waist $w_0 \approx 3$ μm (value evaluated from the diffraction of the ordinary wave component) and $\mathbf{k} \parallel \hat{z}$. The values of birefringence in the near infrared are $\Delta n \approx 0.06$, 0.2 and 0.4 for the three NLC, respectively, with $n_\perp \approx 1.5$ for all of them [60, 61]. Linear and nonlinear parameters of the samples were measured through the beam evolution in the yz plane versus input power P, imaging the scattered light out of yz with a high resolution CCD camera and an optical microscope. Figure 6 shows the light evolution in the three samples for various initial powers, whereas Fig. 7 plots the corresponding trajectories and waists, in good agreement with the numerical results. From the measured trajectories (Fig. 6), the linear walk-off angles for increasing anisotropy resulted in $\delta_0 \approx 2.5°$, 6.5° and 12° [the walk-off is the slope of the curves in Fig. 7(a)], in agreement with the theoretical predictions (Fig. 2). The self-steering predicted in the nonperturbative regime was not observed due to the insurgence of thermal effects and the instabilities stemming from the fluid-like nature of the NLC [21, 58].

Self-confinement was studied by measuring the waist in propagation: at low power, namely $P \approx 0.1$ mW, all three samples exhibited a linear behavior, with diffraction determined by the effective extraordinary index n_{eff} [see (4) and Fig. 2(b)], as visible from the slopes of the solid lines in Fig. 7(b). The nonlinear effects in the low birefringent

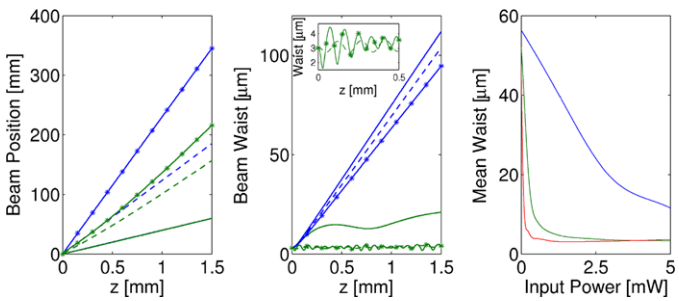

Fig. 5 *Left panel*: beam trajectories in $x = L/2$ for $\Delta n = 0.4$ (*solid lines with symbols*), 0.2 (*dashed lines*) and 0.06 (*solid lines*); for a given NLC, the top *blue* (*bottom green*) line corresponds to $P_{2D} = 1$ μW (4 mW). *Center panel*: beam waist versus z; line types as in the *left panel*. *Inset*: magnification near the input interface, showing the two curves corresponding to $P_{2D} = 4$ mW and $\Delta n = 0.2, 0.4$. *Right panel*: mean beam waist $\overline{w}$ versus excitation for $\Delta n = 0.4$ (*bottom red line*), 0.2 (*middle green line*) and 0.06 (*top blue line*). The parameters are as in Fig. 4

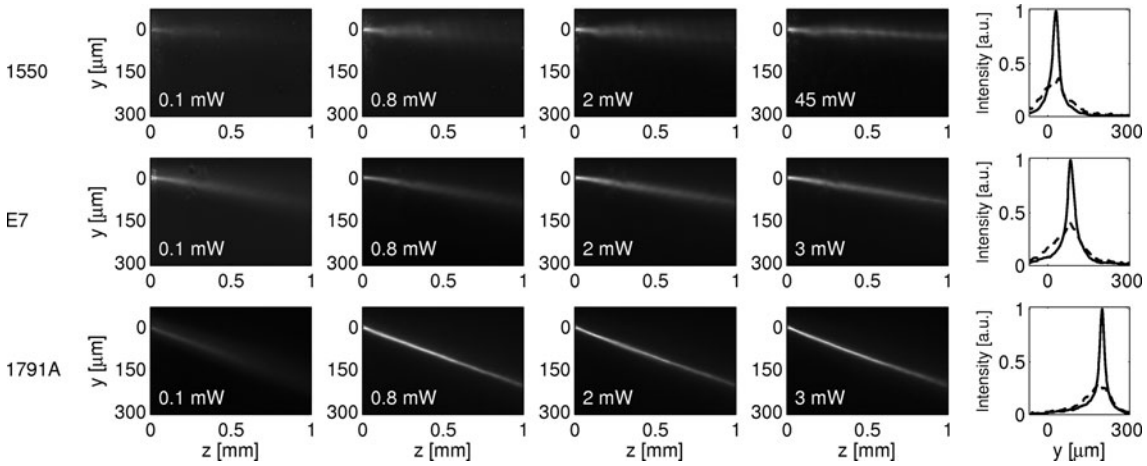

Fig. 6 *First four columns* from the *left*: acquired images of beam evolution for several input powers and three NLC mixtures (see legend on the *left*). *Rightmost plots*: intensity profile at $z = 1$ mm in the linear regime ($P = 0.1$ mW, *dashed lines*) and in the solitonic case (*solid lines*, in the *top graph* $P = 45$ mW, whereas in the *center* and *bottom graphs* $P = 3$ mW)

1550 NLC (Fig. 6 first row) were limited to self-focusing at $P = 3$ mW: as a matter of fact, in Fig. 7(b) the waist increase with z at $P = 3$ mW (blue dashed line) is slightly less than in the linear case ($P = 0.1$ mW, solid blue line). Finally, light self-trapping and the formation of a soliton took place at powers of about 45 mW (Fig. 6, first row, fourth column). In the mixtures $E7$ and $1791A$ (second and third rows in Fig. 6, respectively) self-focusing is stronger owing to the higher ϵ_a, as demonstrated by a direct comparison between the first three columns in Fig. 6. Soliton formation in $E7$ occurred for $P \approx 3$ mW (Fig. 6, second row) consistently with values reported in literature, while for the mixture $1791A$ the minimum power required to observe a soliton was about 800 μW (last row second column in Fig. 6). Remarkably, the experiments confirm the dependence of the nonlinearity on the square of ϵ_a [see Sect. 2, (8)]; in fact, the minimum soliton power in $E7$ is about four times bigger than in $1791A$, in agreement with Δn in $1791A$ being twice larger Δn in $E7$. Similarly, the minimum soliton power is about 15 times larger in 1550 than in $E7$ due to a four times larger anisotropy. We stress that, in such a comparison, using the same effective elastic constants for all the mixtures is a valid assumption because, according to (8), the nonlinear coefficient n_{2H} depends on ϵ_a^2/K. Since the optical anisotropy is known in each NLC mixture and the measured nonlinear effect scales with its square, the effective scalar constant K can be assumed equal in all three samples. The use of one single elastic constant is consistent with other approximations implicitly invoked by our model of nematicon propagation, e.g. scattering losses.

Finally, we pinpoint that the different nonlinearities of $E7$ and $1791A$ are also witnessed by the different breathing periods at fixed power [the case $P = 3$ mW is shown in Fig. 7(b)], with faster oscillations in $1791A$ due to its higher birefringence.

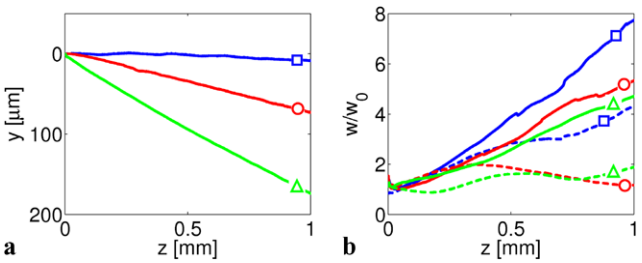

Fig. 7 (**a**) Measured beam trajectories in the plane yz and (**b**) normalized waist w/w_0 (input waist $w_0 \approx 3$ μm) versus z for 1550 ($\Delta n = 0.06$, *blue squares*), $E7$ ($\Delta n = 0.2$, *red circles*) and $1791A$ ($\Delta n = 0.4$, *green triangles*) mixtures. In (**a**) the measured linear walk-off angles are $\delta \approx 2.5°$, 6.5°, 12°, respectively. In (**b**) the *solid lines* correspond to $P = 0.1$ mW and the *dashed lines* to $P = 3$ mW

5 Conclusions

We investigated the role of material parameters in the generation and propagation of spatial optical solitons in nematic liquid crystals. We studied theoretically the behavior of linear and self-confined waves versus refractive indices, evaluating the properties of nematicons and their dependence on birefringence through the introduction of an equivalent nonlocal Kerr parameter. Numerical simulations based on a two-dimensional model and encompassing the main physics confirm our theoretical findings, allowing a more direct comparison with experiments where the input profiles are fixed and the scattering losses are unavoidable. We carried out experimental characterization of three NLC samples featuring different birefringences, obtaining a good agreement with theoretical and numerical results. Our findings demonstrate the

validity of the theoretical tools developed for nematicons, and our results address for the first time the role of physical parameters (dielectric tensor and intermolecular elastic forces) in light self-trapping and self-guiding, enabling to optimize the choice of materials based on the specific applications to be implemented.

Acknowledgements We thank R. Dabrowski for some of the material samples, and E. Nowinowski for preparing the cells. A.A. thanks Regione Lazio for financial support. M. Kwasny visited NooEL in the framework of the European Social Fund through the Warsaw University of Technology Development Programme.

References

1. R.W. Boyd, S.G. Lukishova, Y.R. Shen (eds.), *Self-focusing: Past and Present* (Springer, New York, 2009)
2. Y.S. Kivshar, G.P. Agrawal, *Optical Solitons* (Academic, San Diego, 2003)
3. C. Conti, G. Assanto, *Encyclopedia of Modern Optics*, vol. 5 (Elsevier, Oxford, 2004), pp. 43–55
4. G. Assanto, J. Mod. Opt. **37**, 855 (1990)
5. R.Y. Chiao, E. Garmire, C.H. Townes, Phys. Rev. Lett. **13**, 479 (1964)
6. P.L. Kelley, Phys. Rev. Lett. **15**, 1005 (1965)
7. A. Barthelemy, S. Maneuf, C. Froehly, Opt. Commun. **55**, 201 (1985)
8. J.S. Aitchison, A.M. Weiner, Y. Silberberg, M.K. Oliver, J.L. Jackel, D.E. Leaird, E.M. Vogel, P.W.E. Smith, Opt. Lett. **15**, 471 (1990)
9. F.W. Dabby, J.R. Whinnery, Appl. Phys. Lett. **13**, 284 (1968)
10. J.E. Bjorkholm, A.A. Ashkin, Phys. Rev. Lett. **32**, 129 (1974)
11. D. Suter, T. Blasberg, Phys. Rev. A **48**, 4583 (1993)
12. C. Rotschild, O. Cohen, O. Manela, M. Segev, T. Carmon, Phys. Rev. Lett. **95**, 213904 (2005)
13. C. Conti, G. Ruocco, S. Trillo, Phys. Rev. Lett. **95**, 183902 (2005)
14. Y. Lamhot, A. Barak, O. Peleg, M. Segev, Phys. Rev. Lett. **105**, 163906 (2010)
15. N.I. Nikolov, D. Neshev, O. Bang, W. Królikowski, Phys. Rev. E **68**, 036614 (2003)
16. G. Assanto, M. Peccianti, IEEE J. Quantum Electron. **39**, 13 (2003)
17. G. Assanto, M. Karpierz, Liq. Cryst. **36**, 1161 (2009)
18. I.C. Khoo, Phys. Rep. **471**, 221 (2009)
19. C. Conti, M. Peccianti, G. Assanto, Phys. Rev. Lett. **92**, 113902 (2004)
20. A. Piccardi, M. Peccianti, G. Assanto, A. Dyadyusha, M. Kaczmarek, Appl. Phys. Lett. **94**, 091106 (2009)
21. F. Simoni, *Nonlinear Optical Properties of Liquid Crystals* (World Scientific, Singapore, 1997)
22. G. Assanto, A. Fratalocchi, M. Peccianti, Opt. Express **15**, 5248 (2007)
23. M.A. Karpierz, Phys. Rev. E **66**, 036603 (2002)
24. M. Peccianti, G. Assanto, A. De Luca, C. Umeton, I.C. Khoo, Appl. Phys. Lett. **77**, 7 (2000)
25. M. Peccianti, C. Conti, G. Assanto, A. De Luca, C. Umeton, Nature **432**, 733 (2004)
26. A. Fratalocchi, G. Assanto, K.A. Brzdakiewicz, M.A. Karpierz, Opt. Lett. **29**, 1530 (2004)
27. A. Fratalocchi, G. Assanto, K.A. Brzdakiewicz, M.A. Karpierz, Opt. Express **13**, 1808 (2005)
28. U.A. Laudyn, M. Kwasny, K. Jaworowicz, K.A. Rutkowska, M.A. Karpierz, G. Assanto, Photon. Lett. Pol. **1**, 7 (2009)
29. U.A. Laudyn, M. Kwasny, M.A. Karpierz, Appl. Phys. Lett. **94**, 091110 (2009)
30. F. Derrien, J.F. Henninot, M. Warenghem, G. Abbate, J. Opt. A, Pure Appl. Opt. **2**, 332 (2000)
31. M. Warenghem, J.F. Blach, J.F. Henninot, J. Opt. Soc. Am. B **25**, 1882 (2008)
32. M. Peccianti, C. Conti, G. Assanto, Phys. Rev. E **68**, 025602 (2003)
33. M. Peccianti, C. Conti, G. Assanto, Opt. Lett. **28**, 2231 (2003)
34. C. Conti, M. Peccianti, G. Assanto, Phys. Rev. E **72**, 066614 (2005)
35. M. Peccianti, G. Assanto, Opt. Lett. **30**, 2290 (2005)
36. M. Peccianti, C. Conti, E. Alberici, G. Assanto, Laser Phys. Lett. **2**, 25 (2005)
37. A. Piccardi, A. Alberucci, N. Tabiryan, G. Assanto, Opt. Lett. **36**, 1456 (2011)
38. A. Piccardi, A. Alberucci, G. Assanto, Electron. Lett. **46**, 790 (2010)
39. M. Peccianti, G. Assanto, Opt. Lett. **26**, 1791 (2001)
40. M. Peccianti, G. Assanto, Opt. Lett. **26**, 1690 (2001)
41. M. Peccianti, G. Assanto, Phys. Rev. E **65**, 035603 (2002)
42. A. Piccardi, U. Bortolozzo, S. Residori, G. Assanto, Opt. Lett. **34**, 737 (2009)
43. M. Peccianti, A. Dyadyusha, M. Kaczmarek, G. Assanto, Nat. Phys. **2**, 737 (2006)
44. S.V. Serak, N.V. Tabiryan, M. Peccianti, G. Assanto, IEEE Photonics Technol. Lett. **18**, 1287 (2006)
45. A. Piccardi, G. Assanto, L. Lucchetti, F. Simoni, Appl. Phys. Lett. **93**, 171104 (2008)
46. G. Assanto, B.D. Skuse, N.F. Smyth, Phys. Rev. A **81**, 063811 (2010)
47. A. Pasquazi, A. Alberucci, M. Peccianti, G. Assanto, Appl. Phys. Lett. **87**, 261104 (2005)
48. A. Alberucci, A. Piccardi, U. Bortolozzo, S. Residori, G. Assanto, Opt. Lett. **35**, 390 (2010)
49. G. Assanto, A.A. Minzoni, N.F. Smyth, A.L. Worthy, Phys. Rev. A **82**, 053843 (2010)
50. Y.V. Izdebskaya, V.G. Shvedov, A.S. Desyatnikov, W. Królikowski, Y.S. Kivshar, Opt. Lett. **35**, 1692 (2010)
51. A. Piccardi, A. Alberucci, G. Assanto, J. Opt. Soc. Am. B **27**, 2398 (2010)
52. A. Piccardi, A. Alberucci, G. Assanto, Phys. Rev. Lett. **104**, 213904 (2010)
53. A. Piccardi, A. Alberucci, U. Bortolozzo, S. Residori, G. Assanto, Appl. Phys. Lett. **96**, 071104 (2010)
54. A. Alberucci, M. Peccianti, G. Assanto, G. Coschignano, A. De Luca, C. Umeton, Opt. Lett. **30**, 1381 (2005)
55. A. Alberucci, A. Piccardi, M. Peccianti, M. Kaczmarek, G. Assanto, Phys. Rev. A **82**, 023806 (2010)
56. A. Alberucci, M. Peccianti, G. Assanto, Opt. Lett. **32**, 2795 (2007)
57. E. Braun, L.P. Faucheux, A. Libchaber, Phys. Rev. A **48**, 611 (1993)
58. A. Piccardi, A. Alberucci, G. Assanto, Appl. Phys. Lett. **96**, 061105 (2010)
59. A. Alberucci, G. Assanto, J. Opt. Soc. Am. B **24**, 2314 (2007)
60. R. Dabrowski, Mol. Cryst. Liq. Cryst. **421**, 121 (2004)
61. J. Li, C.-H. Wen, S. Gauza, R. Lu, S.-T. Wu, J. Disp. Technol. **1**, 51 (2005)